

Impact of nonextensivity on the transport coefficients of strongly interacting QCD matter

Dhananjay Singh* and Arvind Kumar†

*Department of Physics, Dr. B R Ambedkar National Institute of Technology Jalandhar,
Jalandhar – 144008, Punjab, India*

Abstract

Tsallis nonextensive statistics is applied to study the transport coefficients of strongly interacting matter within the Polyakov chiral SU(3) quark mean field model (PCQMF). Nonextensivity is introduced within the PCQMF model through a dimensionless q parameter to examine the viscous properties such as shear viscosity (η), bulk viscosity (ζ_b), and conductive properties, including electrical conductivity (σ_{el}) and thermal conductivity (κ). Additionally, some key thermodynamic quantities relevant to the transport coefficients, like the speed of sound (c_{sq}^2) and specific heat at constant volume (c_{vq}), are calculated. The temperature dependence of the transport coefficients is explored through a kinetic theory approach with the relaxation time approximation. The results are compared to the extensive case where q approaches 1. The nonextensive q parameter is found to have a significant effect on all transport coefficients. We find that the nonextensive behaviour of the medium enhances both specific shear viscosity η/s_q as well as conductive coefficients σ_{el}/T and κ/T^2 . In contrast, the normalised bulk viscosity ζ_b/s_q is found to decrease as the nonextensivity of the medium increases. We have also studied the transport coefficients for finite values of chemical potentials. The magnitude of η , σ_{el} , and κ increases at lower temperatures while ζ is found to decrease for systems with non-zero chemical potential.

* snaks16aug@gmail.com

† kumara@nitj.ac.in

I. INTRODUCTION

Relativistic heavy-ion collision experiments offer a distinct opportunity to reproduce the extreme state of matter that existed at the universe's beginning, known as quark-gluon plasma (QGP). Experiments conducted at facilities like the Large Hadron Collider (LHC) at the European Organization for Nuclear Research (CERN) [1–3] and the Relativistic Heavy Ion Collider (RHIC) at Brookhaven National Laboratory (BNL) [4–7] have provided substantial evidence for the creation of QGP which has significantly advanced the exploration and understanding of the strongly interacting matter properties under extreme conditions of temperatures. Additionally, the Beam Energy Scan (BES) initiative at RHIC [8, 9], along with current research programs at the Facility for Antiproton and Ion Research (FAIR) [10, 11] and the Nuclotron-based Ion Collider Facility (NICA) [12, 13], are working to explore the characteristics of baryon-rich nuclear matter.

The role of transport coefficients is crucial for describing the evolution of the bulk matter created in relativistic heavy-ion collisions. These coefficients provide insight into how much a system deviates from ideal hydrodynamics and reveal important information about fluid dynamics and critical phenomena [14–18]. Extracting these coefficients accurately from experimental data and evaluating them using various theoretical approaches is a prominent area of research today. The shear viscosity (η) of hot quantum chromodynamics (QCD) matter has garnered significant interest, primarily because of the surprisingly small value of the ratio of shear viscosity and entropy density, $\eta/s_q = 1/4\pi$, which may resemble a nearly perfect fluid [19]. This finding has led to speculation about the existence of a strongly interacting quark-gluon plasma (sQGP). However, the bulk viscosity to entropy density ratio, ζ_b/s_q , has been suggested to increase near the critical temperature T_c [20–22]. The decreasing value of η/s_q and an increasing value ζ_b/s_q near T_c is found to be consistent with the lattice calculations [23, 24]. The electrical conductivity σ_{el} is important for explaining the enhancement of low-mass dimuons [25] and serves as an essential input for magnetohydrodynamic simulations [26, 27]. Another key transport coefficient for hydrodynamic evolution at finite chemical potential is thermal conductivity κ , which has been explored in Refs. [28–31]. These collective findings emphasise that transport coefficients play an important role in measuring the properties of strongly interacting relativistic QCD matter and understanding its phase transitions [15].

In recent years, transport coefficients have been extensively studied using a variety of effective QCD [32–37] and hadronic models [38–45]. However, these models employ a statistical approach based on the Boltzmann-Gibbs (BG) statistics, which is valid only for systems having strong dynamical correlations, homogeneous and infinite heat bath, long-range interactions, and microscopic memory effects [46–50]. However, in the initial stages of the heavy ion collision experiments, these conditions are rarely met. Hence, some quantities develop power-law-tailed distributions and become nonextensive. To address these issues, Tsallis proposed nonextensive statistics as a generalization of the BG statistics by introducing a dimensionless q parameter to account for all potential variables that violate the assumptions of the standard BG statistics [46]. In this framework, Tsallis proposed a generalized non-additive entropy

$$s_q = \frac{1 - \sum_{i=1}^w P_i^q}{q - 1}, \quad (1)$$

where w is the number of microstates, P_i is the probability distribution with $\sum_{i=1}^w P_i = 1$, and q is a positive real number called the nonextensive q -parameter. Assuming equiprobability ($P_i = 1/w$), the Tsallis entropy in Eq. (1) reduces to [46, 51]

$$s_q = \frac{w^{1-q} - 1}{1 - q} = \ln_q w, \quad (2)$$

here the q -logarithm is defined as [52]

$$\ln_q(x) \equiv \frac{x^{1-q} - 1}{1 - q}, \quad (3)$$

with corresponding q -exponential expressed as

$$\exp_q(x) = [1 + (1 - q)x]^{1/(1-q)}. \quad (4)$$

The non-additivity of the entropy s_q follows from the non-additivity of the q -logarithm [46]: considering two independent systems A and B with $P_{(A+B)} = P_A P_B$, the generalized entropy of the system takes the form

$$s_q(A + B) = s_q(A) + s_q(B) + (1 - q)s_q(A)s_q(B). \quad (5)$$

The quantity $|1 - q|$ quantifies the degree of the non-equilibration, i.e., how far the system is away from equilibrium. For $q > 1$, it describes intrinsic fluctuations of temperature in the system [53, 54]. In Ref. [55], it was observed that temperature fluctuations are measured by the divergence of q from unity, while the Boltzmann limit ($q = 1$) does not

show any temperature fluctuation. Thus, utilizing the nonextensive Tsallis statistics within the dynamical model is highly advantageous for examining the transport coefficients as they are not well-defined during the initial stage of heavy-ion collisions where the system is in non-equilibrium. In the present work, we attempt to see possible deviations from standard BG statistics for the values of $q > 1$, as these values have been seen in numerous phenomenological investigations of high-energy heavy ion collisions [55–57]. In the limit $q \rightarrow 1$, the nonextensive entropy reduces to the usual BG entropy, i.e., $s_{q=1} = s_{BG}$. The q -parameter is incorporated into the specific dynamical formulas of the model and enables a straightforward phenomenological test against possible deviations from the BG framework.

Tsallis nonextensive statistics has gained considerable importance in recent years due to its ability to fit transverse momentum distributions across a broad range of collision energies, as demonstrated by the STAR [58], PHENIX [59], ALICE [60], and CMS [61] collaborations. In light of this, nonextensivity has been incorporated into many theoretical models to study the properties of the QCD matter. These include a generalized Quantum Hydrodynamics (q -QHD) model [62], a nonextensive version of Nambu-Jona-Lasinio (q -NJL) model [63], a nonextensive version of MIT bag (q -MIT) model [64], a generalized linear sigma model (q -LSM) [65], and a nonextensive Polyakov chiral SU(3) quark mean field (q -PCQMF) model [66]. Recently, the q -PNJL model has been employed to study the transport coefficients [67], critical exponents [68], and fluctuations in the baryon number [69]. Nonextensivity has also been incorporated within the relaxation time approximation of kinetic theory to study the viscous coefficients [70] and conductive coefficients [71] of hot and dense magnetized QCD matter. Furthermore, the bulk properties of protoneutron stars [72] and the thermodynamics of a black hole [73] have also been explored using nonextensive statistics.

In the present study, we aim to utilise the q -PCQMF to investigate the transport coefficients of strongly interacting QCD matter at finite temperatures and chemical potentials. We study the temperature variations of the transport coefficients using the expressions obtained from kinetic theory and the relaxation time approximation at zero and finite values of chemical potentials. Additionally, we have included the presence of quark back reaction by replacing the usual Polyakov loop potential with the QCD glue potential [74, 75]. This is done by substituting the pure gauge temperature T_{YM} with the glue potential temperature T_{glue} . This paper is organized as follows: In Sec. II, we give a brief introduction of the

nonextensive version of the Polyakov chiral SU (3) quark mean field (q -PCQMF) model. Sec. III discusses the expressions of the transport coefficients. The impact of the q -parameter on the transport coefficients of strongly interacting QCD matter is discussed in Sec. IV. Finally, our brief summary and conclusions are presented in Sec. V.

II. q -PCQMF MODEL

The thermodynamic potential density of the q -extended Polyakov chiral SU(3) quark mean field model in the mean field approximation is defined as [66]

$$\Omega_q = \mathcal{U}(\Phi, \bar{\Phi}, T) - \mathcal{L}_M - \mathcal{V}_{vac} + \sum_{i=u,d,s} \frac{-\gamma_i k_B T}{(2\pi)^3} \int_0^\infty d^3k \{ \ln_q F_q^- + \ln_q F_q^+ \}, \quad (6)$$

where $\mathcal{L}_M = \mathcal{L}_{\Sigma\Sigma} + \mathcal{L}_{VV} + \mathcal{L}_{SB}$ is the meson interaction term. In this model, the attractive part of the interactions between quarks is represented by scalar meson fields σ , ζ , and δ while the repulsive part is represented by vector fields ρ , ω and ϕ . The Polyakov loop fields Φ and $\bar{\Phi}$ are included in the model to study deconfinement phase transition. Additionally, the model incorporates broken scale invariance by introducing a scalar dilaton field, χ [76–78]. For the scalar meson, the self-interaction term $\mathcal{L}_{\Sigma\Sigma}$ is expressed in terms of the scalar fields as

$$\begin{aligned} \mathcal{L}_{\Sigma\Sigma} = & -\frac{1}{2} k_0 \chi^2 (\sigma^2 + \zeta^2 + \delta^2) + k_1 (\sigma^2 + \zeta^2 + \delta^2)^2 + k_2 \left(\frac{\sigma^4}{2} + \frac{\delta^4}{2} + 3\sigma^2 \delta^2 + \zeta^4 \right) \\ & + k_3 \chi (\sigma^2 - \delta^2) \zeta - k_4 \chi^4 - \frac{1}{4} \chi^4 \ln \frac{\chi^4}{\chi_0^4} + \frac{d}{3} \chi^4 \ln \left(\left(\frac{(\sigma^2 - \delta^2) \zeta}{\sigma_0^2 \zeta_0} \right) \left(\frac{\chi^3}{\chi_0^3} \right) \right), \end{aligned} \quad (7)$$

where $\sigma_0 = -f_\pi$ and $\zeta_0 = \frac{1}{\sqrt{2}}(f_\pi - 2f_K)$ correspond to the vacuum values of σ and ζ field, where $f_\pi = 93$ MeV and $f_K = 115$ MeV are the pion and kaon decay constant, respectively. The value of $d = 6/33$ is chosen to produce the correct trace anomaly for three flavours and three colours of quarks [79]. The vector meson self-interaction term is given by

$$\mathcal{L}_{VV} = \frac{1}{2} \frac{\chi^2}{\chi_0^2} (m_\omega^2 \omega^2 + m_\rho^2 \rho^2 + m_\phi^2 \phi^2) + g_4 (\omega^4 + 6\omega^2 \rho^2 + \rho^4 + 2\phi^4), \quad (8)$$

with $m_\phi = 1020$ MeV is the ϕ meson mass and $m_\omega = m_\rho = 783$ MeV is the mass of ω and ρ meson. Finally, the spontaneous symmetry-breaking term \mathcal{L}_{SB} is written as [80]

$$\mathcal{L}_{SB} = -\frac{\chi^2}{\chi_0^2} \left[m_\pi^2 f_\pi \sigma + \left(\sqrt{2} m_K^2 f_K - \frac{m_\pi^2}{\sqrt{2}} f_\pi \right) \zeta \right]. \quad (9)$$

The term $\mathcal{U}(\Phi, \bar{\Phi}, T)$ in Eq. (6) is the Polyakov loop effective potential, which in the logarithmic form is given by [81, 82]

$$\frac{\mathcal{U}(\Phi, \bar{\Phi})}{T^4} = -\frac{a(T)}{2}\bar{\Phi}\Phi + b(T)\ln[1 - 6\bar{\Phi}\Phi + 4(\bar{\Phi}^3 + \Phi^3) - 3(\bar{\Phi}\Phi)^2], \quad (10)$$

where

$$a(T) = a_0 + a_1\left(\frac{T_0}{T}\right) + a_2\left(\frac{T_0}{T}\right)^2, \quad b(T) = b_3\left(\frac{T_0}{T}\right)^3, \quad (11)$$

with $a_0 = 1.81$, $a_1 = -2.47$, $a_2 = 15.2$ and $b_3 = -1.75$ [83]. Incorporating the effects of the backreaction of quarks leads to substituting the Polyakov loop potential with the QCD glue potential [74]. Denoting the Polyakov loop potential in Eq. (10) as \mathcal{U}_{YM} , the improved glue Polyakov loop potential \mathcal{U}_{glue} is written as [75]

$$\frac{\mathcal{U}_{glue}(\Phi, \bar{\Phi}, T_{glue})}{T_{glue}} = \frac{\mathcal{U}_{YM}(\Phi, \bar{\Phi}, T_{YM})}{T_{YM}}, \quad (12)$$

with $T = T_0^{YM} \left(1 + 0.57 \left(\frac{T_{glue}}{T_0^{glue}-1}\right)\right)$ and $T_0 = T_0^{YM}$ in the RHS of the Eq. (10). In the present work, we have taken $T_0^{YM} = T_0^{glue} = 200$ MeV. In the last term of Eq. (6), $\gamma_i = 2$ is the spin degeneracy factor, and

$$F_q^- = 1 + \exp_q(-3E^-) + 3\Phi \exp_q(-E^-) + 3\bar{\Phi} \exp_q(-2E^-), \quad (13)$$

$$F_q^+ = 1 + \exp_q(-3E^+) + 3\bar{\Phi} \exp_q(-E^+) + 3\Phi \exp_q(-2E^+), \quad (14)$$

where $E^- = (E_i^*(k) - \mu_i^*)/k_B T$ and $E^+ = (E_i^*(k) + \mu_i^*)/k_B T$ and $E_i^*(k) = \sqrt{m_i^{*2} + k^2}$ represents the effective energy of quarks. The in-medium quark chemical potential μ_i^* can be written in terms of quark chemical potential μ_i as $\mu_i^* = \mu_i - g_\omega^i \omega - g_\phi^i \phi - g_\rho^i \rho$. Here, g_ω^i , g_ϕ^i and g_ρ^i are the coupling coefficients between vector meson fields and various quarks. The in-medium mass of quarks $m_i^* = -g_\sigma^i \sigma - g_\zeta^i \zeta - g_\delta^i \delta + \Delta m_i$, with g_σ^i , g_ζ^i , and g_δ^i represent the coupling constants between scalar meson fields and various quarks and $\Delta m_{u,d} = 0$ and $\Delta m_s = 29$ MeV. The term \mathcal{V}_{vac} in Eq. (6) is subtracted to get zero vacuum energy. The temperature dependence of the scalar and vector fields is obtained by minimizing the thermodynamic potential density in Eq. (6) with respect to these fields, i.e.,

$$\frac{\partial \Omega_q}{\partial \sigma} = \frac{\partial \Omega_q}{\partial \zeta} = \frac{\partial \Omega_q}{\partial \delta} = \frac{\partial \Omega_q}{\partial \chi} = \frac{\partial \Omega_q}{\partial \omega} = \frac{\partial \Omega_q}{\partial \rho} = \frac{\partial \Omega_q}{\partial \phi} = \frac{\partial \Omega_q}{\partial \Phi} = \frac{\partial \Omega_q}{\partial \bar{\Phi}} = 0. \quad (15)$$

The resulting coupled equations are provided in the Appendix. The vector density $\rho_{q,i}$ and the scalar density $\rho_{q,i}^s$ in the q -PCQMF model are defined as

$$\rho_{q,i} = \gamma_i N_c \int \frac{d^3 k}{(2\pi)^3} \left(f_{q,i}(k) - \bar{f}_{q,i}(k) \right), \quad (16)$$

and

$$\rho_{q,i}^s = \gamma_i N_c \int \frac{d^3k}{(2\pi)^3} \frac{m_i^*}{E_i^*(k)} \left(f_{q,i}(k) + \bar{f}_{q,i}(k) \right), \quad (17)$$

respectively, with q -modified Fermi-distribution functions for quarks and antiquarks

$$f_{q,i}(k) = \frac{\Phi \exp_q^q(-E^-) + 2\bar{\Phi} \exp_q^q(-2E^-) + \exp_q^q(-3E^-)}{[1 + 3\Phi \exp_q(-E^-) + 3\bar{\Phi} \exp_q(-2E^-) + \exp_q(-3E^-)]^q}, \quad (18)$$

$$\bar{f}_{q,i}(k) = \frac{\bar{\Phi} \exp_q^q(-E^+) + 2\Phi \exp_q^q(-2E^+) + \exp_q^q(-3E^+)}{[1 + 3\bar{\Phi} \exp_q(-E^+) + 3\Phi \exp_q(-2E^+) + \exp_q(-3E^+)]^q}, \quad (19)$$

respectively.

It is crucial to mention that as q approaches 1, the standard Fermi-distribution functions are restored, leading us back to the conventional (extensive) PCQMF model. Additionally, as temperature, $T \rightarrow 0$, the q -dependent thermodynamic potential density Ω_q defined in Eq. (6) also returns to its standard (extensive) form defined in Ref. [83], as long as $q > 1$. This implies that the nonextensive effects are more prominent in heavy-ion collision experiments where the temperature reaches a few orders of MeVs and the value of q remains greater than 1 [84–86].

The parameters of the model used in the present study are summarized in Table I. These are adjusted to accurately reproduce the vacuum masses of π , K , σ , ζ , χ , and the average masses of η and η' [79]. The relations of the baryon, isospin, and strangeness chemical potential are defined as

$$\mu_B = \frac{3}{2}(\mu_u + \mu_d), \quad (20)$$

$$\mu_I = \frac{1}{2}(\mu_u - \mu_d), \quad (21)$$

$$\mu_S = \frac{1}{2}(\mu_u + \mu_d - 2\mu_s), \quad (22)$$

respectively. Here, μ_u , μ_d , and μ_s represent the chemical potentials of up, down, and strange quarks, respectively.

III. TRANSPORT COEFFICIENTS

Transport coefficients for a system in the hydrodynamic regime can be determined using the Kubo formalism [87, 88], assuming that the relaxation time is shorter than the system's lifetime. The expressions for the transport coefficients obtained using this formalism are

k_0	k_1	k_2	k_3	k_4	g_s	g_v	g_4	d	$\rho_0(\text{fm}^{-3})$
4.94	2.12	-10.16	-5.38	-0.06	4.76	6	37.5	0.18	0.15
σ_0 (MeV)	ζ_0 (MeV)	χ_0 (MeV)	m_π (MeV)	f_π (MeV)	m_K (MeV)	f_K (MeV)	m_ω (MeV)	m_ϕ (MeV)	m_ρ (MeV)
-93	-96.87	254.6	139	93	496	115	783	1020	783
g_σ^u	g_σ^d	g_σ^s	g_ζ^u	g_ζ^d	g_ζ^s	g_δ^u	g_δ^d	g_δ^s	g_ω^u
3.36	3.36	0	0	0	4.76	3.36	-3.36	0	3.86
g_ω^d	g_ω^s	g_ϕ^u	g_ϕ^d	g_ϕ^s	g_ρ^u	g_ρ^d	g_ρ^s		
3.86	0	0	0	5.46	3.86	-3.86	0		

TABLE I. The list of parameters used in the present work [79].

identical to those derived within a quasiparticle approach in kinetic theory using the relaxation time approximation (RTA) [90, 91]. In kinetic theory, the transport coefficients are derived using the Boltzmann transport equation, which can be written in the relaxation time approximation (RTA) as

$$k^\mu \partial_\mu f_i = C[f], \quad (23)$$

where $C[f]$ is the collision integral. To study the transport coefficients, we are interested in small departures of the distribution function from the equilibrium,

$$\delta f_i(\vec{x}, \vec{k}, t) = f'_i(\vec{x}, \vec{k}, t) - f_i(\vec{x}, \vec{k}, t). \quad (24)$$

Here f_i is the local equilibrium distribution of quarks, and f'_i is the non-equilibrium distribution function. Under nonextensive statistics, the equilibrium distributions are modified to their q -modified versions. This results in q -generalized transport equation known as nonextensive Boltzmann transport equation (NEBE) [92],

$$k^\mu \partial_\mu f_{q,i} = C_q[f], \quad (25)$$

with $C_q[f]$ being the q -deformed collision term. In Ref. [89], authors demonstrated that it is valid to employ conventional methods for calculating transport coefficients, beginning with NEBE. These computations yield relations for all transport coefficients that are formally analogous to those derived from the conventional Boltzmann-Gibbs distributions. The expressions of various transport coefficients used in the present work are presented below

[88, 93, 94]:

$$\eta = \frac{2N_c}{15T} \sum_{i=u,d,s} \int \frac{d^3k}{(2\pi)^3} \tau \left(\frac{k^2}{E_i^*} \right)^2 [f_{q,i}(1 - f_{q,i}) + \bar{f}_{q,i}(1 - \bar{f}_{q,i})], \quad (26)$$

$$\zeta_b = \frac{2N_c}{T} \sum_{i=u,d,s} \int \frac{d^3k}{(2\pi)^3} \tau \frac{1}{E_i^{*2}} \left[\left(\frac{1}{3} - c_{sq}^2 \right) k^2 - c_{sq}^2 m_i^{*2} + c_{sq}^2 m_i^* T \frac{dm_i^*}{dT} \right]^2 [f_{q,i}(1 - f_{q,i}) + \bar{f}_{q,i}(1 - \bar{f}_{q,i})], \quad (27)$$

$$\sigma_{el} = \frac{2N_c}{3T} \sum_{i=u,d,s} e_i^2 \int \frac{d^3k}{(2\pi)^3} \tau \left(\frac{k}{E_i^*} \right)^2 [f_{q,i}(1 - f_{q,i}) + \bar{f}_{q,i}(1 - \bar{f}_{q,i})], \quad (28)$$

$$\kappa = \frac{2N_c}{3T^2} \sum_{i=u,d,s} \int \frac{d^3k}{(2\pi)^3} \tau \left(\frac{k}{E_i^*} \right)^2 [(E_i^* - h_q)^2 f_{q,i}(1 - f_{q,i}) + (E_i^* + h)^2 \bar{f}_{q,i}(1 - \bar{f}_{q,i})]. \quad (29)$$

Notably, $f_{q,i}$ and $\bar{f}_{q,i}$ are not the standard Fermi-distribution functions but rather the q -version of the Fermi-distribution functions, given by Eqs. (18) and (19). c_{sq}^2 is the speed of sound at constant entropy defined as $c_{sq}^2 = (\partial p_q / \partial \epsilon_q)_{s_q} = s_q / c_{vq}$ and c_{vq} is the specific heat at constant volume defined as $c_{vq} = (\partial \epsilon_q / \partial T)_{V}$. The pressure is given by $p_q = -\Omega_q$ while the energy density and the entropy density are defined as $\epsilon_q = \Omega_q + \sum_{i=u,d,s} \mu_i^* \rho_i + T s_q$ and $s_q = -\partial \Omega_q / \partial T$, respectively. The heat function $h_q = (\epsilon_q + p_q) / \rho_q$ diverges at $\mu = 0$ where ρ_q diverges. The relaxation time τ is the measure of the timescale over which the distribution function relaxes back to equilibrium and is defined as [95]

$$\tau = \frac{1}{5.1T\alpha_s^2 \log(\frac{1}{\alpha_s})(1 + 0.12(2N_f + 1))}, \quad (30)$$

where α_s is the temperature and chemical potential dependent strong coupling constant given by [96, 97]

$$\alpha_s(T, \mu) = \frac{6\pi}{(33 - 2N_f) \log\left(\frac{T}{\Lambda_T} \sqrt{1 + \left(\frac{\mu}{\pi T}\right)^2}\right)} \left(1 - \frac{3(153 - 19N_f) \log\left(2 \log\frac{T}{\Lambda_T} \sqrt{1 + \left(\frac{\mu}{\pi T}\right)^2}\right)}{(33 - 2N_f)^2 \log\left(\frac{T}{\Lambda_T} \sqrt{1 + \left(\frac{\mu}{\pi T}\right)^2}\right)} \right), \quad (31)$$

with $\Lambda_T = 70$ MeV [97].

IV. RESULTS AND DISCUSSIONS

In this section, we will discuss the impact of the nonextensive q parameter on the thermodynamic quantities and transport coefficients of strongly interacting QCD matter within the q -PCQMF model presented in Sec. II. The q -PCQMF model incorporates the influence of the q parameter through the thermodynamic potential density, Ω_q . This modification of the potential density results in modification of the scalar density, $\rho_{q,i}^s$, and vector density, $\rho_{q,i}$, of constituent quarks. These densities, in turn, modifies the scalar ($\sigma, \zeta, \delta, \chi$), vector (ω, ρ, ϕ), and Polyakov loop fields ($\Phi, \bar{\Phi}$) which are determined by solving the interconnected system of non-linear equations given in Appendix.

Let us start by examining how the nonextensive q parameter impacts the scalar fields σ and ζ . Figure 1 displays the changes in the scalar fields σ and ζ , with respect to temperature T , while keeping the baryon chemical potentials μ_B fixed at 0 and 600 MeV, respectively. The values of q used are 1, 1.05, and 1.10. It is evident that the magnitude of σ and ζ fall as the temperature of the medium rises. The decrease in the amplitude of scalar fields may indicate the restoration of chiral symmetry at elevated temperatures. As the temperature rises, the Fermi distribution function described by Eqs. (18) and (19) decreases, leading to a reduction in the magnitude of the scalar fields. As the value of q becomes greater than 1, at a certain temperature T , the scalar fields σ and ζ experience a decrease in magnitude. For example, at zero baryon chemical potential and temperature $T = 200$ MeV, the magnitude of the σ (ζ) field decreases from 38.97 MeV (72.49 MeV) at $q = 1$ to 34.49 MeV (67.27 MeV) and 30.34 MeV (61 MeV) as the value of $q = 1.05$ and 1.10, respectively. This indicates that the restoration of chiral symmetry at higher temperatures is faster for systems with a higher degree of nonextensivity, i.e., higher q . Additionally, in subplots (b) and (d) of Fig. 1, temperature variations of the scalar fields σ and ζ are shown at a finite value of the baryon chemical potential $\mu_B = 600$ MeV, isospin chemical potential $\mu_I = -30$ MeV, and strangeness chemical potential $\mu_S = 125$ MeV, for $q = 1, 1.05, \text{ and } 1.10$. At low temperatures, when the baryon chemical potential is raised from zero to a non-zero value, we notice a drop in the magnitude of the scalar fields. At temperature $T = 120$ MeV and $q = 1$, as the baryon chemical potential is increased from 0 to 600 MeV, the magnitude of the σ (ζ) field decreases from 93.1 MeV (98.2 MeV) to 76.73 MeV (92.51 MeV), respectively. Again, increasing the degree of nonextensivity, i.e., the magnitudes of $\sigma(\zeta)$ decrease to 70.22 MeV

(90.11 MeV) and 64.46 MeV (87.75 MeV) for $q = 1.05$ and 1.10 , respectively. Ultimately, we can deduce that the chiral symmetry restoration shifts to lower temperatures as the value of baryon chemical potential becomes finite.

The order parameters used to investigate deconfinement in the mean-field approximation are the Polyakov loop fields, denoted as Φ and $\bar{\Phi}$. Temperature variations in the magnitude of Φ and $\bar{\Phi}$ provide insights into the deconfinement phase transition. Figure 2 shows the Polyakov fields Φ and $\bar{\Phi}$ as a function of temperature T , with baryon chemical potential set at $\mu_B = 0$ and 600 MeV, for $q = 1, 1.05,$ and 1.10 . At zero baryon chemical potential, in subplots (a) and (c) of Fig. 2, we observe that the values of Φ and $\bar{\Phi}$ are almost zero at lower temperatures, suggesting the presence of confined quarks within hadrons. As the temperature increases, quarks transition from being confined to becoming deconfined, and the values of Φ and $\bar{\Phi}$ become nonzero. Like scalar fields, we observe that as nonextensivity grows (with greater values of q), the increase in Φ and $\bar{\Phi}$ happens earlier. This suggests a reduction in the temperature at which deconfinement occurs for values of q greater than 1. For a finite baryon chemical potential of $\mu_B = 600$ MeV (Figs. 2(b) and 2(d)), the Polyakov fields, Φ and $\bar{\Phi}$, have non-zero values even at lower temperatures. This may imply that quarks become deconfined at lower temperatures for non-zero values of baryon chemical potential. In conclusion, increasing nonextensivity or baryon chemical potential results in shifting the deconfinement temperature to lower values.

Next, we discuss the impact of the q parameter on the in-medium masses of quarks. Figure 3 shows the temperature variations of effective masses of quarks m_u^*, m_d^* , and m_s^* at baryon chemical potentials $\mu_B = 0$ and 600 MeV, for $q = 1, 1.05,$ and 1.10 . The in-medium effective quark masses are dependent on the in-medium scalar fields. As discussed in Fig. 1, the magnitude of the scalar fields σ and ζ decreases as the temperature of the medium is raised. This results in the fall of the effective quark masses with a rise in temperature. This may be attributed to the transition of quarks from within the confined state of hadrons to a state of deconfined QGP at higher temperatures. For a given temperature, we observe that increasing the nonextensivity ($q > 1$) results in a decrease in the effective quark masses. Again, this may be indicative that the chiral symmetry restoration is shifted to lower temperatures with increasing nonextensivity in the system, as was discussed in Fig. 1. As for the case of finite baryon chemical potential of $\mu_B = 600$ MeV (subplots (b), (d), and (f) of Fig. 3), we find that the quark masses are reduced even at lower temperature values. Also, due to a finite

value of isospin chemical potential $\mu_I = -30$ MeV, there is a minor difference in the effective masses of u and d quarks. For example, at $T = 200$ MeV and $q = 1$, we find the effective mass of u quark to be $m_u^* \approx 123$ MeV while $m_d^* \approx 119$ MeV. For values of q greater than 1, we observe these values to decrease more sharply, indicating a quicker restoration of chiral symmetry for systems with a higher degree of nonextensivity.

Figure 4 showcase the changes in scaled thermodynamic quantities: ϵ_q/T^4 , p_q/T^4 , s_q/T^3 , and $(\epsilon_q - 3p_q)/T^4$, as temperature T varies. The results are shown for both zero and as well as finite value of baryon chemical potential at $q = 1, 1.05$, and 1.10 . All of these quantities remain insignificant at low temperatures, but they increase when the system approaches the transition point. At high temperatures, the interaction among quarks weakens, causing the thermodynamic properties to approach the ideal gas limit or the Stefan-Boltzmann (SB) limit [83, 98]. Notably, for $q = 1$, all of them stay under their respective SB limit at high temperatures. However, when $q > 1$, we find that these thermodynamic quantities grow rapidly and go beyond their respective SB limits at higher temperatures. A similar impact of nonextensivity was observed on the thermodynamic quantities in the PNJL model [67]. This is a consequence of using Tsallis statistics in the model. As when $T \rightarrow \infty$, the q -modified potential density Ω_q does not converge to its standard value Ω . This means that for systems with $q > 1$, the thermodynamic quantities at the high T limit are pushed beyond their corresponding SB limit and approach a new Tsallis limit. For a non-zero value of baryon chemical potential ($\mu_B = 600$ MeV), we can see from subplots (b), (d), (f), and (h) in Fig. 4 that the thermodynamic quantities start to have non-zero values even at lower temperatures. Again, increasing q from 1 to 1.10 results in a rise in the magnitude of these quantities, similar to the case of vanishing baryon chemical potential.

In Fig. 5, we plot the scaled specific heat c_{vq}/T^3 and the speed of sound c_{sq}^2 as a function of temperature T at baryon chemical potentials $\mu_B = 0$ and 600 MeV, for $q = 1, 1.05$, and 1.10 . For the case of vanishing μ_B , we find that c_{vq}/T^3 exhibits a similar pattern to the other thermodynamic quantities. For $q = 1$, it rises sharply near the transition temperature and reaches its SB limit at higher temperatures. For $q > 1$, we observe that c_{vq}/T^3 surpasses its SB limit and reaches a higher Tsallis limit at high T . In subplot (d) of Fig. 5, we observe that for non-zero μ_B , the rise in c_{vq}/T^3 occurs at much lower temperatures before saturating to a constant value at higher temperatures. As for the speed of sound, c_{sq}^2 , we find that it reaches a minimum near the transition temperature and then increases to reach its SB limit at high

T . We observe that the dip becomes less prominent, and its position is shifted towards lower temperatures as $q > 1$. Additionally, for a fixed T , its value increases with increasing q . However, unlike the thermodynamic quantities discussed so far, c_{sq}^2 remains within the SB limit for all values of q studied in the present work. This happens as $c_{sq}^2 = s_q/c_{vq}$, and both s_q and c_{vq} exhibit comparable increase at high temperature. This results in c_{sq}^2 always remaining under the SB limit. In addition, we find that the dip in c_{sq}^2 vanishes when the baryon chemical potential is increased to $\mu_B = 600$ MeV, as can be seen in Fig. 5(d).

In Figs. 6(a) and (b), we have shown the dependence of the speed of sound squared c_{sq}^2 and scaled specific heat c_{vq}/T^3 on the baryon chemical potential μ_B , for $q = 1, 1.05$, and 1.10 and temperatures $T = 90$ and 150 MeV. The plots are shown for zero value of strangeness chemical potential μ_S , isospin chemical potential μ_I and vector coupling constant g_v . For $q = 1$ and $T = 90$ MeV, we observe that c_{sq}^2 starts from a low value at smaller μ_B and shows a dip before rising as μ_B increases. The dip in c_{sq}^2 may indicate the position of pseudo-critical temperature for chiral phase transition in the $T - \mu_B$ phase diagram [99]. We find that as the value of q is increased to 1.05 and 1.10 , the dip shifts to lower values of μ_B . This may signify a shift in the chiral transition to lower chemical potentials for nonextensive systems. An increase in the value of temperature also shifts the dip in c_{sq}^2 to lower values of μ_B . Similar kind of behaviour is also observed for the scaled specific heat c_{vq}/T^3 in Fig. 6(b). For $T = 90$ MeV, we find that c_{vq}/T^3 starts from a low value and rises with increasing baryon chemical potential before showing a peak at higher μ_B . Increasing the value of q shifts the position of the peak to lower μ_B . At higher temperature of $T = 150$ MeV, the peak in c_{vq}/T^3 disappears.

Let us now begin the discussion of the viscous transport coefficients of the QCD matter. Shear viscosity η and bulk viscosity ζ_b serve as important parameters to describe the hydrodynamical evolution of the QCD medium, thereby impacting phenomenological observables such as correlation functions and elliptical flow [16, 100]. In subplots (a) and (b) of Fig. 7, we present the temperature dependence of the shear viscosity to entropy ratio η/s_q in the q -PCQMF model for the value of $q = 1, 1.05$, and 1.10 . The results are shown for baryon chemical potentials $\mu_B = 0$ and 600 MeV. At vanishing baryon chemical potential, η/s_q approaches the KSS bound ($1/4\pi$) and shows a minimum near the transition temperature and increases slowly thereafter. For temperatures below the transition temperature, η/s_q grows and diverges as $T \rightarrow 0$. This is similar to the findings observed in the PNJL model [35, 93].

Beyond the transition temperature, η/s_q grows slowly and exhibits similarities to a fluid experiencing a phase change from liquid to gas [101]. As for the impact of the q parameter on η/s_q , we find that its reaction to q increases with temperature. The effective constituent quark mass decreases with temperature, leading to an increase in the value of η/s_q at high temperatures. This decrease in the effective quark masses is more for systems with higher nonextensivity, i.e., $q > 1$. Hence, resulting in an enhanced value of η/s_q for $q > 1$. This is similar to the observations in the q -PNJL model [67] where η is increased for values of $q > 1$. In Ref. [70], η/s_q is found to have a little increase due to the nonextensive behaviour of the medium. Also, we find that the magnitude of the minima in η/s_q increases for higher q values. We observe the qualitative nature of η/s_q remains the same, and the magnitude of the minima is increased for the value of baryon chemical potential $\mu_B = 600$ MeV. The effect of increasing q remains the same as in the case of vanishing chemical potential.

Fig. 7(c) and (d) shows the bulk viscosity to entropy density ratio ζ_b/s_q as a function of temperature T with baryon chemical potential fixed at $\mu_B = 0$ and 600 MeV, for $q = 1, 1.05,$ and 1.10 . The bulk viscosity is an important parameter, especially due to its connection to the conformal symmetry of the system [102]. At low temperatures, ζ_b/s_q is large due to the comparative magnitudes of ζ_b and s_q . For $\mu_B = 0$ MeV, we note that ζ_b/s_q shows a slight peak close to the transition temperature and then slowly decreases to zero at higher temperatures. This vanishing value of ζ_b/s_q can be explained by the significant increase in s_q relative to ζ_b , suggesting that the system achieves conformal symmetry at high temperatures. The PNJL model [103] and the PLSM model [37] also show a similar trend for ζ_b/s_q . Increasing the nonextensivity ($q > 1$), we find that the peak in ζ_b/s_q disappears as it gradually goes to zero at high T . Additionally, unlike η/s_q , we find that the normalised bulk viscosity ζ_b/s_q decreases as the nonextensivity of the medium is increased. This is similar to the findings in Ref. [70]. The decreasing value of ζ_b/s_q indicates that the system gets closer to the conformal limit as the degree of nonextensivity of the medium is increased. Furthermore, at finite baryon chemical potential of $\mu_B = 600$ MeV, we observe that ζ_b/s_q shows no peak, and its magnitude gets smaller as can be seen in subplot (d) of Fig. 7. In addition, we observe that increasing the value of q results in a slight increase in ζ_b/s_q at lower temperatures, while a slight decrease at higher temperatures.

Now, we come to the discussion of the conductive transport coefficients, namely, the electrical conductivity σ_{el} and the thermal conductivity κ in the q -PCQMF model. In Fig,

8, we show temperature variation of σ_{el}/T for both zero as well as the finite value of baryon chemical potential at $q = 1, 1.05, \text{ and } 1.10$. The electrical conductivity σ_{el} serves as a vital tool to understand the electromagnetic interactions in QCD matter. For $\mu_B = 0$ MeV, we find σ_{el} to increase with temperature T . This can be attributed to the deconfinement of quarks at high T , allowing them to move around easily and enhance electrical conductivity. The NJL model [88] and PNJL model [93] report similar findings for σ_{el}/T . Regarding the impact of nonextensivity q on σ_{el}/T , we observe that increasing q results in increased electrical conductivity, even at lower temperatures. The electrical conductivity, σ_{el} , is found to increase with the introduction of nonextensivity in the kinetic theory approach [71] and in the q -PNJL model [67]. This may be due to a decrease in the effective quark mass for the system with higher nonextensivity ($q > 1$). Another reason could be the tendency of the quarks to become deconfined at lower temperatures for nonextensive systems, as was pointed out in Fig. 2. Increasing the baryon chemical potential μ_B to 600 MeV results in an increased magnitude of σ_{el}/T at lower temperatures. We find σ_{el}/T to increase with the rise in the degree of nonextensivity ($q > 1$), similar to the case of $\mu_B = 0$ MeV.

We have also computed the thermal conductivity κ/T^2 , which is associated with the heat flow of the QGP. In Fig. 9, we plot κ/T^2 as a function of T for $\mu_B = 600$ MeV, $\mu_I = -30$ MeV, $\mu_S = 125$ MeV, at $q = 1, 1.05, \text{ and } 1.10$. According to Eq. (29), κ/T^2 diverges at $\mu_B = 0$ MeV due to the diverging nature of the heat function h at vanishing chemical potential. As the temperature of the system increases, the value of h increases, leading to an efficient transmission of heat within the QGP, thereby enhancing thermal conductivity. As for the impact of the q parameter, we find that similar to other transport coefficients, κ/T^2 increases for $q > 1$ with the influence more noticeable in the high T region. Again, this is similar to the observations in Ref. [71].

Finally, we have shown the baryon chemical potential dependence of the transport coefficients in Fig. 10 for different values of q at temperatures $T = 150$ and 200 MeV and $\mu_S = \mu_I = g_v = 0$. In Fig. 10(a), we find that η/s_q increases with increasing value of μ_B . The value of η/s_q is found to increase with increasing nonextensivity in the system (higher q values). A contrasting behaviour is observed in ζ_b/s_q , which is found to decrease with increasing μ_B and q , as shown in Fig. 10(b). Also, we find that increasing the temperature results in lower values of ζ_b/s_q , suggesting conformal symmetry restoration. As for the electrical conductivity σ_{el}/T in Fig. 10(c), we find that it starts from a low value and rises with

μ_B . While the thermal conductivity κ/T^2 is observed to start from a higher value at small μ_B and decreases with increasing μ_B as shown in Fig. 10(d). The high value of κ/T^2 at small μ_B is due to its diverging nature at $\mu_B = 0$ as pointed out earlier. As for the impact of nonextensivity, we observe that both electrical and thermal conductivity increases for higher q values and the influence is more prominent at lower μ_B .

V. SUMMARY AND CONCLUSION

In this study, we have used the nonextensive Polyakov chiral SU(3) quark mean field (q -PCQMF) model for three quark flavours (u, d, s) to calculate the transport coefficients such as the shear η and bulk viscosity ζ_b as well as the electrical σ_{el} and thermal conductivity κ as a function of temperature T . We have evaluated the transport coefficients for both zero and finite baryon chemical potential ($\mu_B = 600$ MeV), taking into account the finite values of isospin ($\mu_I = -30$ MeV) and strangeness chemical potentials ($\mu_S = 125$ MeV). The value of the nonextensivity parameter q used are 1, 1.05., and 1.10. In order to examine the transport coefficients while taking into account the nonextensivity, we have computed the q -dependent thermodynamic quantities such as pressure density p_q/T^4 , energy density ϵ_q/T^4 , entropy density s_q/T^3 , trace anomaly $(\epsilon_q - 3p_q)/T^4$, speed of sound squared c_{sq}^2 , and specific heat c_{vq}/T^3 . We find that at higher temperatures, all thermodynamic quantities except c_{sq}^2 approach the q -dependent Tsallis limit instead of their usual SB limit. Due to an unexpected cancellation, the high-temperature limit of c_{sq}^2 remains unaffected. We also found that the effective quark masses decrease as the nonextensivity of the system increases, possibly due to the shift of chiral symmetry restoration to lower temperatures. For vanishing baryon chemical potential, the temperature variation of the ratio of shear viscosity to entropy density η/s_q shows that it approaches the KSS bound and a minimum near the transition temperature, rising thereafter. On the other hand, the bulk viscosity to entropy ratio ζ_b/s_q exhibits a small peak near the transition temperature and vanishes at higher temperatures. Furthermore, we find that both the electrical conductivity σ_{el} and the thermal κ conductivity increase monotonically with temperature. Regarding the impact of the nonextensive q parameter, we find that the transport coefficients η/s_q , σ_{el}/T , and κ/T^2 get enhanced while ζ_b/s_q get diminished for systems with $q > 1$. The impact of nonextensivity on the transport coefficients is found to be more prominent in the high T

range. In addition, we have also studied all the transport coefficients at finite values of chemical potentials. We found that increasing the chemical potentials leads to a larger magnitude of the transport coefficients at lower temperatures, possibly owing to the early restoration of chiral symmetry for systems with finite density. In future, we aim to utilise the q -PCQMF model to study the transport coefficient in a magnetised nonextensive QCD medium.

VI. ACKNOWLEDGMENT

The authors sincerely acknowledge the support toward this work from the Ministry of Science and Human Resources (MHRD), Government of India, via an Institute fellowship under the Dr B R Ambedkar National Institute of Technology Jalandhar.

APPENDIX

The coupled equations are obtained by minimizing the thermodynamic potential density, Ω_q , with respect to the various fields of the q -PCQMF model and are given as

$$\begin{aligned}
\frac{\partial \Omega_q}{\partial \sigma} &= k_0 \chi^2 \sigma - 4k_1 (\sigma^2 + \zeta^2 + \delta^2) \sigma - 2k_2 (\sigma^3 + 3\sigma\delta^2) - 2k_3 \chi \sigma \zeta \\
&- \frac{d}{3} \chi^4 \left(\frac{2\sigma}{\sigma^2 - \delta^2} \right) + \left(\frac{\chi}{\chi_0} \right)^2 m_\pi^2 f_\pi - \left(\frac{\chi}{\chi_0} \right)^2 m_\omega \omega^2 \frac{\partial m_\omega}{\partial \sigma} \\
&- \left(\frac{\chi}{\chi_0} \right)^2 m_\rho \rho^2 \frac{\partial m_\rho}{\partial \sigma} - \sum_{i=u,d} g_\sigma^i \rho_{q,i}^s = 0,
\end{aligned} \tag{32}$$

$$\begin{aligned}
\frac{\partial \Omega_q}{\partial \zeta} &= k_0 \chi^2 \zeta - 4k_1 (\sigma^2 + \zeta^2 + \delta^2) \zeta - 4k_2 \zeta^3 - k_3 \chi (\sigma^2 - \delta^2) - \frac{d}{3} \frac{\chi^4}{\zeta} \\
&+ \left(\frac{\chi}{\chi_0} \right)^2 \left[\sqrt{2} m_K^2 f_K - \frac{1}{\sqrt{2}} m_\pi^2 f_\pi \right] - \left(\frac{\chi}{\chi_0} \right)^2 m_\phi \phi^2 \frac{\partial m_\phi}{\partial \zeta} - \sum_{i=s} g_\zeta^i \rho_{q,i}^s \\
&= 0,
\end{aligned} \tag{33}$$

$$\begin{aligned}
\frac{\partial \Omega_q}{\partial \delta} &= k_0 \chi^2 \delta - 4k_1 (\sigma^2 + \zeta^2 + \delta^2) \delta - 2k_2 (\delta^3 + 3\sigma^2 \delta) + 2k_3 \chi \delta \zeta \\
&+ \frac{2}{3} d \chi^4 \left(\frac{\delta}{\sigma^2 - \delta^2} \right) - \sum_{i=u,d} g_\delta^i \rho_{q,i}^s = 0,
\end{aligned} \tag{34}$$

$$\begin{aligned}
\frac{\partial \Omega_q}{\partial \chi} &= k_0 \chi (\sigma^2 + \zeta^2 + \delta^2) - k_3 (\sigma^2 - \delta^2) \zeta + \chi^3 \left[1 + \ln \left(\frac{\chi^4}{\chi_0^4} \right) \right] + (4k_4 - d) \chi^3 \\
&- \frac{4}{3} d \chi^3 \ln \left(\left(\frac{(\sigma^2 - \delta^2) \zeta}{\sigma_0^2 \zeta_0} \right) \left(\frac{\chi}{\chi_0} \right)^3 \right) + \frac{2\chi}{\chi_0^2} \left[m_\pi^2 f_\pi \sigma + \left(\sqrt{2} m_K^2 f_K - \frac{1}{\sqrt{2}} m_\pi^2 f_\pi \right) \zeta \right] \\
&- \frac{\chi}{\chi_0^2} (m_\omega^2 \omega^2 + m_\rho^2 \rho^2) = 0,
\end{aligned} \tag{35}$$

$$\frac{\partial \Omega_q}{\partial \omega} = \frac{\chi^2}{\chi_0^2} m_\omega^2 \omega + 4g_4 \omega^3 + 12g_4 \omega \rho^2 - \sum_{i=u,d} g_\omega^i \rho_{q,i} = 0, \tag{36}$$

$$\frac{\partial \Omega_q}{\partial \rho} = \frac{\chi^2}{\chi_0^2} m_\rho^2 \rho + 4g_4 \rho^3 + 12g_4 \omega^2 \rho - \sum_{i=u,d} g_\rho^i \rho_{q,i} = 0, \tag{37}$$

$$\frac{\partial \Omega_q}{\partial \phi} = \frac{\chi^2}{\chi_0^2} m_\phi^2 \phi + 8g_4 \phi^3 - \sum_{i=s} g_\phi^i \rho_{q,i} = 0, \tag{38}$$

$$\begin{aligned}
\frac{\partial \Omega_q}{\partial \Phi} &= \left[\frac{-a(T) \bar{\Phi}}{2} - \frac{6b(T)(\bar{\Phi} - 2\bar{\Phi}^2 + \bar{\Phi}^2 \Phi)}{1 - 6\bar{\Phi} \Phi + 4(\bar{\Phi}^3 + \Phi^3) - 3(\bar{\Phi} \Phi)^2} \right] T^4 - \sum_{i=u,d,s} \frac{2k_B T N_C}{(2\pi)^3} \\
&\int_0^\infty d^3 k \left[\frac{\exp_q \left(\frac{-(E_i^*(k) - \mu_i^*)}{k_B T} \right)}{\left(1 + \exp_q \left(\frac{-3(E_i^*(k) - \mu_i^*)}{k_B T} \right) + 3\Phi \exp_q \left(\frac{-(E_i^*(k) - \mu_i^*)}{k_B T} \right) + 3\bar{\Phi} \exp_q \left(\frac{-2(E_i^*(k) - \mu_i^*)}{k_B T} \right) \right)^q} \right. \\
&\quad \left. + \frac{\exp_q \left(\frac{-2(E_i^*(k) + \mu_i^*)}{k_B T} \right)}{\left(1 + \exp_q \left(\frac{-3(E_i^*(k) + \mu_i^*)}{k_B T} \right) + 3\bar{\Phi} \exp_q \left(\frac{-(E_i^*(k) + \mu_i^*)}{k_B T} \right) + 3\Phi \exp_q \left(\frac{-2(E_i^*(k) + \mu_i^*)}{k_B T} \right) \right)^q} \right] \\
&= 0 \tag{39}
\end{aligned}$$

and

$$\begin{aligned}
\frac{\partial \Omega_q}{\partial \bar{\Phi}} &= \left[\frac{-a(T) \Phi}{2} - \frac{6b(T)(\Phi - 2\bar{\Phi}^2 + \Phi^2 \bar{\Phi})}{1 - 6\bar{\Phi} \Phi + 4(\bar{\Phi}^3 + \Phi^3) - 3(\bar{\Phi} \Phi)^2} \right] T^4 - \sum_{i=u,d,s} \frac{2k_B T N_C}{(2\pi)^3} \\
&\int_0^\infty d^3 k \left[\frac{\exp_q \left(\frac{-2(E_i^*(k) - \mu_i^*)}{k_B T} \right)}{\left(1 + \exp_q \left(\frac{-3(E_i^*(k) - \mu_i^*)}{k_B T} \right) + 3\Phi \exp_q \left(\frac{-(E_i^*(k) - \mu_i^*)}{k_B T} \right) + 3\bar{\Phi} \exp_q \left(\frac{-2(E_i^*(k) - \mu_i^*)}{k_B T} \right) \right)^q} \right. \\
&\quad \left. + \frac{\exp_q \left(\frac{-(E_i^*(k) + \mu_i^*)}{k_B T} \right)}{\left(1 + \exp_q \left(\frac{-3(E_i^*(k) + \mu_i^*)}{k_B T} \right) + 3\bar{\Phi} \exp_q \left(\frac{-(E_i^*(k) + \mu_i^*)}{k_B T} \right) + 3\Phi \exp_q \left(\frac{-2(E_i^*(k) + \mu_i^*)}{k_B T} \right) \right)^q} \right] \\
&= 0 \tag{40}
\end{aligned}$$

-
- [1] K. Aamodt *et al.* [ALICE], Phys. Rev. Lett. **105**, 252301 (2010).
- [2] S. Chatrchyan *et al.* [CMS], JHEP **08**, 141 (2011).
- [3] K. Aamodt *et al.* [ALICE], Phys. Lett. B **696**, 30-39 (2011).
- [4] I. Arsene *et al.* [BRAHMS], Nucl. Phys. A **757**, 1-27 (2005).
- [5] B. B. Back *et al.* [PHOBOS], Nucl. Phys. A **757**, 28-101 (2005).
- [6] K. Adcox *et al.* [PHENIX], Nucl. Phys. A **757**, 184-283 (2005).
- [7] J. Adams *et al.* [STAR], Nucl. Phys. A **757**, 102-183 (2005).
- [8] B. Mohanty [STAR], J. Phys. G **38**, 124023 (2011).
- [9] L. Adamczyk *et al.* [STAR], Phys. Rev. C **96**, no.4, 044904 (2017).
- [10] N. A. Tahir, C. Deutsch, V. E. Fortov *et al.* Phys. Rev. Lett. **95**, 035001 (2005).
- [11] T. Ablyazimov *et al.* [CBM], Eur. Phys. J. A **53**, no.3, 60 (2017).
- [12] B. Friman *et al.* “The CBM physics book: Compressed baryonic matter in laboratory experiments,” Lect. Notes Phys. **814**, pp.1-980 (2011).
- [13] V. Kekelidze, R. Lednicky, V. Matveev *et al.* Phys. Part. Nucl. Lett. **9**, 313-316 (2012).
- [14] P. Kovtun, D. T. Son and A. O. Starinets, Phys. Rev. Lett. **94**, 111601 (2005).
- [15] L. P. Csernai, J. I. Kapusta and L. D. McLerran, Phys. Rev. Lett. **97**, 152303 (2006).
- [16] P. Romatschke and U. Romatschke, Phys. Rev. Lett. **99**, 172301 (2007).
- [17] A. Muronga, Phys. Rev. C **76**, 014909 (2007).
- [18] R. S. Bhalerao, Pramana **75**, 247-258 (2010).
- [19] R. A. Lacey, N. N. Ajitanand, J. M. Alexander *et al.* Phys. Rev. Lett. **98**, 092301 (2007).
- [20] K. Paech and S. Pratt, Phys. Rev. C **74**, 014901 (2006).
- [21] D. Kharzeev and K. Tuchin, JHEP **09**, 093 (2008).
- [22] F. Karsch, D. Kharzeev and K. Tuchin, Phys. Lett. B **663**, 217-221 (2008).
- [23] A. Nakamura and S. Sakai, Phys. Rev. Lett. **94**, 072305 (2005).
- [24] H. B. Meyer, Phys. Rev. Lett. **100**, 162001 (2008).
- [25] P. Mohanty, S. Ghosh and S. Mitra, Adv. High Energy Phys. **2013**, 176578 (2013).
- [26] V. Roy, S. Pu, L. Rezzolla and D. Rischke, Phys. Lett. B **750**, 45-52 (2015).
- [27] V. Roy, S. Pu, L. Rezzolla and D. H. Rischke, Phys. Rev. C **96**, no.5, 054909 (2017).
- [28] G. S. Denicol, H. Niemi, E. Molnar *et al.* Phys. Rev. D **85**, 114047 (2012).

- [29] M. Greif, F. Reining, I. Bouras *et al.* Phys. Rev. E **87**, 033019 (2013).
- [30] G. S. Denicol, H. Niemi, I. Bouras *et al.* Phys. Rev. D **89**, no.7, 074005 (2014).
- [31] J. I. Kapusta and J. M. Torres-Rincon, Phys. Rev. C **86**, 054911 (2012).
- [32] R. Marty, E. Bratkovskaya, W. Cassing *et al.* Phys. Rev. C **88**, 045204 (2013).
- [33] P. Deb, G. P. Kadam and H. Mishra, Phys. Rev. D **94**, no.9, 094002 (2016).
- [34] C. Sasaki and K. Redlich, Nucl. Phys. A **832**, 62-75 (2010).
- [35] S. K. Ghosh, S. Raha, R. Ray *et al.* Phys. Rev. D **91**, no.5, 054005 (2015).
- [36] S. Ghosh, T. C. Peixoto, V. Roy *et al.* Phys. Rev. C **93**, no.4, 045205 (2016).
- [37] A. N. Tawfik, A. M. Diab and M. T. Hussein, Int. J. Mod. Phys. A **31**, no.34, 1650175 (2016).
- [38] D. Fernandez-Fraile and A. Gomez Nicola, Eur. Phys. J. C **62**, 37-54 (2009).
- [39] K. Itakura, O. Morimatsu and H. Otomo, Phys. Rev. D **77**, 014014 (2008).
- [40] R. Lang, N. Kaiser and W. Weise, Eur. Phys. J. A **48**, 109 (2012).
- [41] S. Mitra, S. Ghosh and S. Sarkar, Phys. Rev. C **85**, 064917 (2012).
- [42] S. Ghosh, G. Krein and S. Sarkar, Phys. Rev. C **89**, no.4, 045201 (2014).
- [43] S. Ghosh, Phys. Rev. C **90**, no.2, 025202 (2014).
- [44] S. Ghosh, Braz. J. Phys. **45**, no.6, 687-698 (2015).
- [45] G. P. Kadam and H. Mishra, Nucl. Phys. A **934**, 133-147 (2014).
- [46] C. Tsallis, J. Stat. Phys. **52**, 479-487 (1988).
- [47] E. M. F. Curado and C. Tsallis, J. Phys. A **24**, L69-L72 (1991).
- [48] C. Tsallis, Phys. World **10**, no. 7, 42 (1997).
- [49] C. Tsallis, "Introduction to Nonextensive Statistical Mechanics: Approaching a Complex World," Springer, 2009.
- [50] T. Kodama and T. Koide, Eur. Phys. J. A **40**, 289-297 (2009).
- [51] K. K. Gudima, A. S. Parvan, M. Ploszajczak *et al.* Phys. Rev. Lett. **85**, 4691-4694 (2000).
- [52] C. Tsallis and Z. G. Arenas, EPJ Web Conf. **71**, 00132 (2014).
- [53] G. Wilk and Z. Wlodarczyk, Phys. Rev. Lett. **84**, 2770 (2000).
- [54] T. S. Biro and G. Purcsel, Phys. Rev. Lett. **95**, 162302 (2005).
- [55] J. Cleymans, G. Hamar, P. Levai *et al.* J. Phys. G **36**, 064018 (2009).
- [56] M. Biyajima, M. Kaneyama, T. Mizoguchi *et al.* Eur. Phys. J. C **40**, 243-250 (2005).
- [57] J. Cleymans and D. Worku, Eur. Phys. J. A **48**, 160 (2012).
- [58] B. I. Abelev *et al.* [STAR], Phys. Rev. C **75**, 064901 (2007).

- [59] A. Adare *et al.* [PHENIX], Phys. Rev. C **83**, 064903 (2011).
- [60] K. Aamodt *et al.* [ALICE], Eur. Phys. J. C **71**, 1655 (2011).
- [61] V. Khachatryan *et al.* [CMS], JHEP **05**, 064 (2011).
- [62] F. I. M. Pereira, R. Silva and J. S. Alcaniz, Phys. Rev. C **76**, 015201 (2007).
- [63] J. Rozynek and G. Wilk, J. Phys. G **36**, 125108 (2009).
- [64] P. H. G. Cardoso, T. Nunes da Silva, A. Deppman *et al.* Eur. Phys. J. A **53**, no.10, 191 (2017).
- [65] K. M. Shen, H. Zhang, D. F. Hou *et al.* Adv. High Energy Phys. **2017**, 4135329 (2017).
- [66] D. Singh and A. Kumar, Chin. Phys. C **48**, no.5, 053103 (2024).
- [67] Y. P. Zhao, Phys. Rev. D **101**, no.9, 096006 (2020).
- [68] Y. P. Zhao, S. Y. Zuo and C. M. Li, Chin. Phys. C **45**, no.7, 073105 (2021).
- [69] Y. P. Zhao, C. Y. Wang, S. Y. Zuo *et al.* Chin. Phys. C **47**, no.5, 053103 (2023).
- [70] S. Rath and S. Dash, Eur. Phys. J. A **60**, no.2, 29 (2024).
- [71] S. Rath and S. Dash, Eur. Phys. J. C **83**, no.9, 867 (2023).
- [72] A. Lavagno and D. Pigato, Eur. Phys. J. A **47**, 52 (2011).
- [73] E. Megias, D. P. Menezes and A. Deppman, Physica A **421**, 15-24 (2015).
- [74] L. M. Haas, R. Stiele, J. Braun *et al.* Phys. Rev. D **87**, no.7, 076004 (2013).
- [75] S. K. Rai and V. K. Tiwari, Phys. Rev. D **109**, no.3, 034025 (2024).
- [76] J. Schechter, Phys. Rev. D **21**, 3393-3400 (1980).
- [77] R. Gomm, P. Jain, R. Johnson *et al.* Phys. Rev. D **33**, 801 (1986).
- [78] E. K. Heide, S. Rudaz and P. J. Ellis, Nucl. Phys. A **571**, 713-732 (1994).
- [79] P. Wang, V. E. Lyubovitskij, T. Gutsche *et al.* Phys. Rev. C **67**, 015210 (2003).
- [80] P. Wang, Z. Y. Zhang, Y. W. Yu *et al.* Nucl. Phys. A **705**, 455-474 (2002).
- [81] K. Fukushima, Phys. Lett. B **591**, 277-284 (2004).
- [82] M. Fukugita, M. Okawa and A. Ukawa, Nucl. Phys. B **337**, 181-232 (1990).
- [83] M. Kumari and A. Kumar, Eur. Phys. J. Plus **136**, no.1, 19 (2021).
- [84] B. C. Li, Y. Z. Wang and F. H. Liu, Phys. Lett. B **725**, 352-356 (2013).
- [85] J. Cleymans, G. I. Lykasov, A. S. Parvan *et al.* Phys. Lett. B **723**, 351-354 (2013).
- [86] M. D. Azmi and J. Cleymans, J. Phys. G **41**, 065001 (2014).
- [87] R. Kubo, J. Phys. Soc. Jap. **12**, 570-586 (1957).
- [88] S. Ghosh, F. E. Serna, A. Abhishek *et al.* Phys. Rev. D **99**, no.1, 014004 (2019).

- [89] T. S. Biró and E. Molnár, *Eur. Phys. J. A* **48**, 172 (2012).
- [90] P. B. Arnold, G. D. Moore and L. G. Yaffe, *JHEP* **11**, 001 (2000).
- [91] P. Chakraborty and J. I. Kapusta, *Phys. Rev. C* **83**, 014906 (2011).
- [92] A. Lavagno, *Physica A* **305**, 238-241 (2002).
- [93] K. Saha, S. Ghosh, S. Upadhaya *et al.* *Phys. Rev. D* **97**, no.11, 116020 (2018).
- [94] C. A. Islam, J. Dey and S. Ghosh, *Phys. Rev. C* **103**, no.3, 034904 (2021).
- [95] A. Hosoya and K. Kajantie, *Nucl. Phys. B* **250**, 666-688 (1985).
- [96] V. M. Bannur, *Phys. Rev. C* **75**, 044905 (2007).
- [97] L. L. Zhu and C. B. Yang, *Nucl. Phys. A* **831**, 49-58 (2009).
- [98] S. Borsanyi, G. Endrodi, Z. Fodor *et al.* *JHEP* **08**, 053 (2012).
- [99] H. Liu, Y. H. Yang, C. Yuan *et al.* *Phys. Rev. D* **109**, no.7, 074037 (2024).
- [100] J. Y. Ollitrault, *Phys. Rev. D* **46**, 229-245 (1992).
- [101] T. Schäfer and D. Teaney, *Rept. Prog. Phys.* **72**, 126001 (2009).
- [102] P. B. Arnold, C. Dogan and G. D. Moore, *Phys. Rev. D* **74**, 085021 (2006).
- [103] K. Saha, S. Upadhaya and S. Ghosh, *Mod. Phys. Lett. A* **32**, no.05, 1750018 (2016).

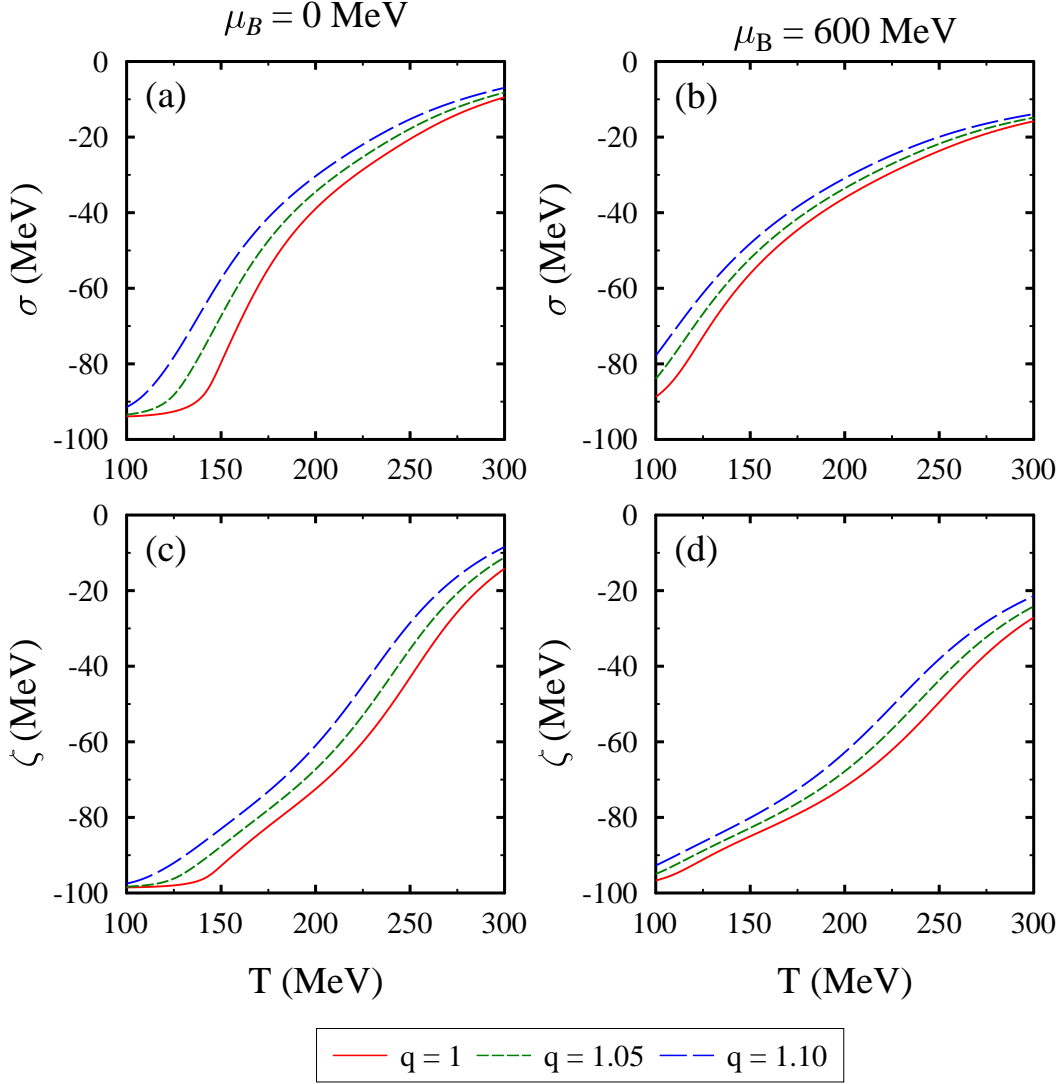


FIG. 1. The scalar fields σ and ζ are plotted as a function of temperature T for the value of nonextensivity parameter $q = 1, 1.05,$ and 1.10 , at baryon chemical potential $\mu_B = 0 \text{ MeV}$ [in subplots (a) and (c)], and baryon chemical potential $\mu_B = 600 \text{ MeV}$, isospin chemical potential $\mu_I = -30 \text{ MeV}$, and strangeness chemical potential $\mu_S = 125 \text{ MeV}$ [in subplots (b) and (d)].

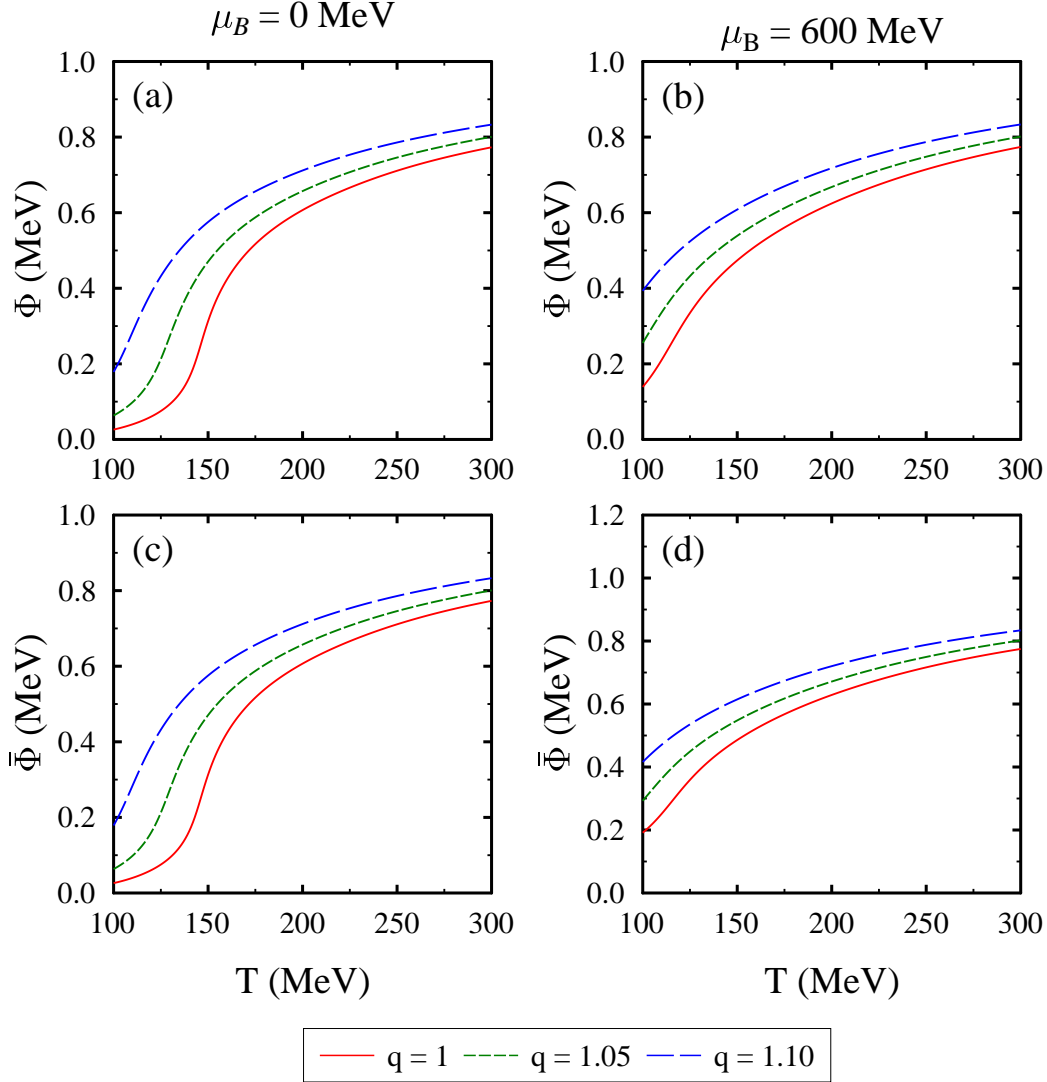


FIG. 2. The Polyakov fields Φ and $\bar{\Phi}$ are plotted as a function of temperature T for the value of nonextensivity parameter $q = 1, 1.05$, and 1.10 , at baryon chemical potential $\mu_B = 0 \text{ MeV}$ [in subplots (a) and (c)], and baryon chemical potential $\mu_B = 600 \text{ MeV}$, isospin chemical potential $\mu_I = -30 \text{ MeV}$, and strangeness chemical potential $\mu_S = 125 \text{ MeV}$ [in subplots (b) and (d)].

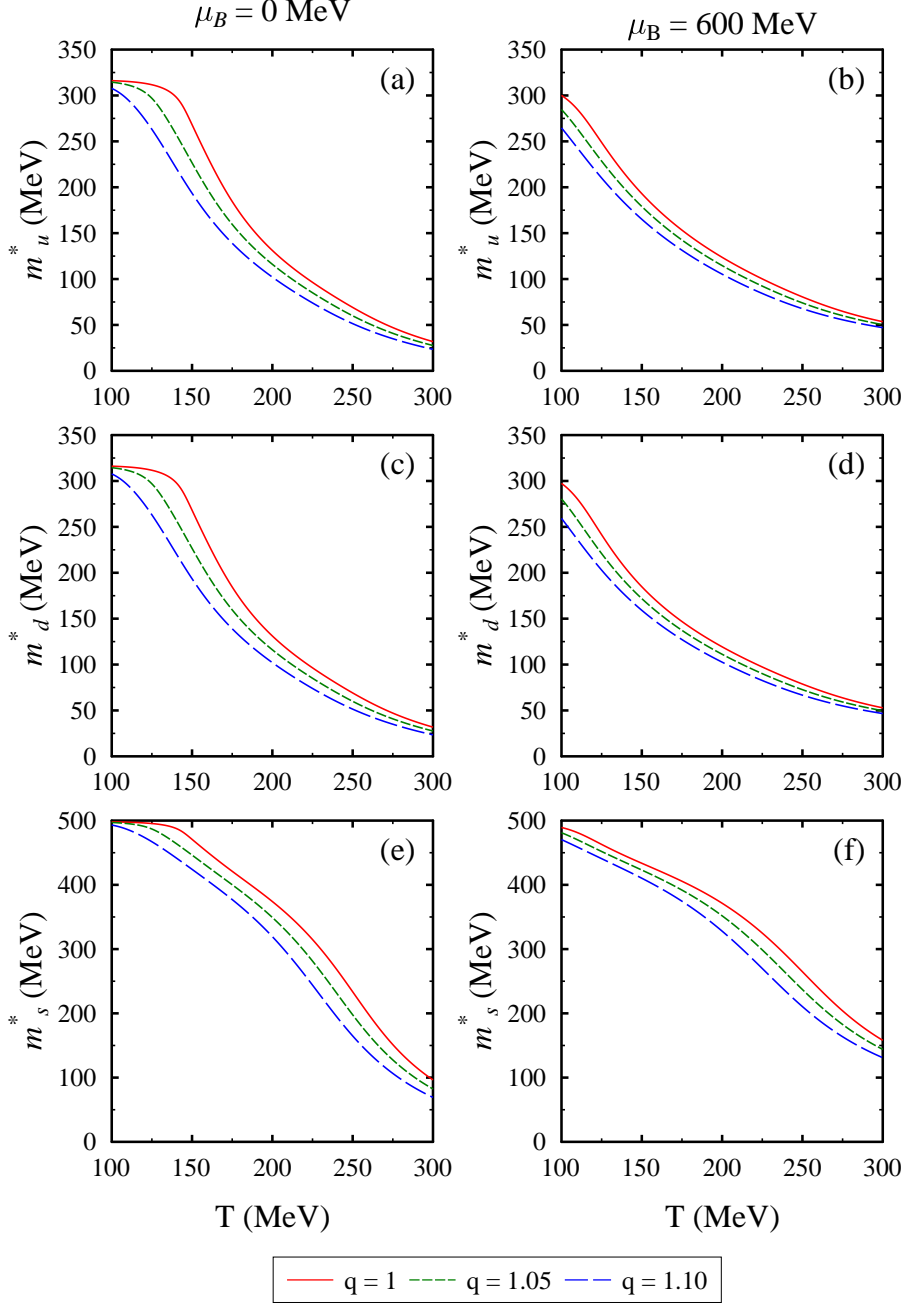


FIG. 3. The effective quark masses m_u^* , m_d^* , and m_s^* plotted as a function of temperature T for the value of nonextensivity parameter $q = 1, 1.05$, and 1.10 , at baryon chemical potential $\mu_B = 0$ MeV [in subplots (a), (c), and (e)], and baryon chemical potential $\mu_B = 600$ MeV, isospin chemical potential $\mu_I = -30$ MeV, and strangeness chemical potential $\mu_S = 125$ MeV [in subplots (b),(d), and (f)].

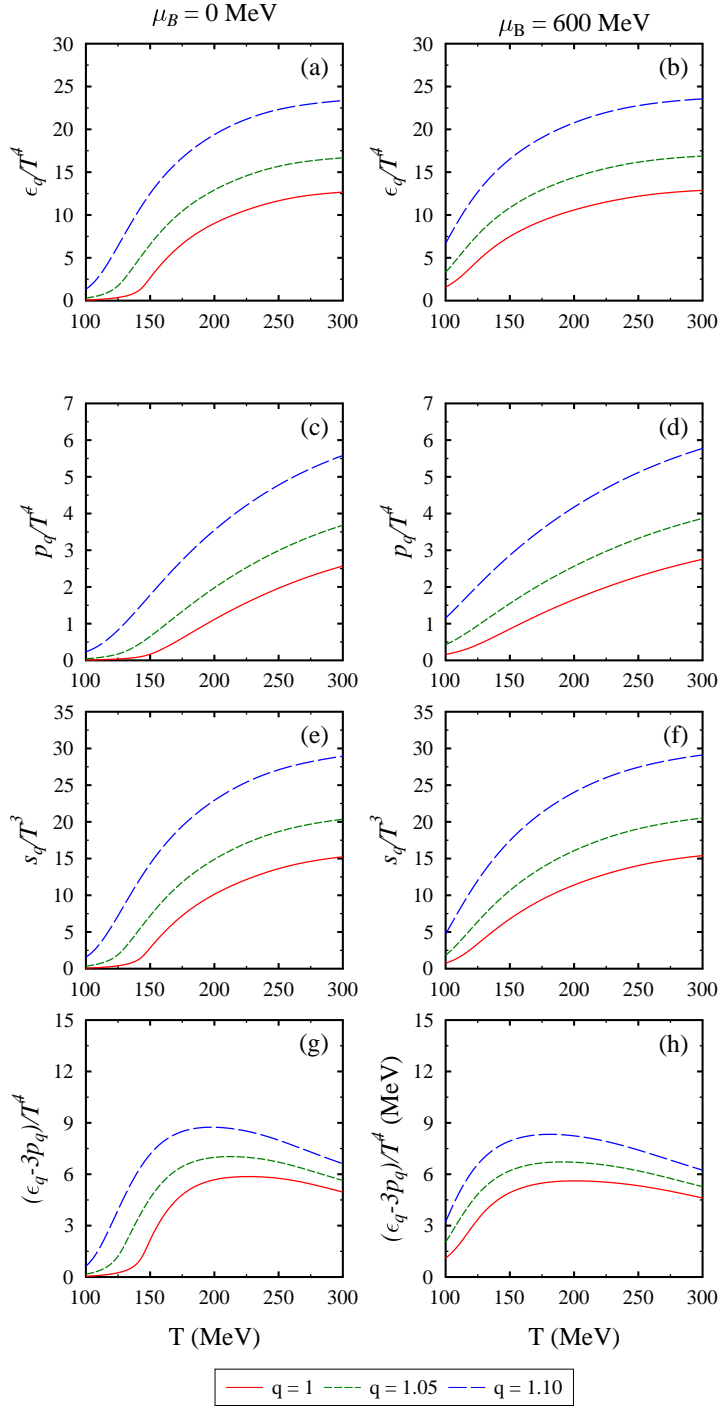


FIG. 4. The scaled pressure density p_q/T^4 , scaled energy density ϵ_q/T^4 , scaled entropy density s_q/T^3 , and trace anomaly $(\epsilon_q - 3p_q)/T^4$ as a function of temperature T for the value of nonextensivity parameter $q = 1, 1.05,$ and 1.10 , at $\mu_B = 0$ MeV [in subplots (a), (c), (e), and (g)] and $\mu_B = 600$ MeV, $\mu_I = -30$ MeV, $\mu_S = 125$ MeV [in subplots (b), (d), (f), and (h)].

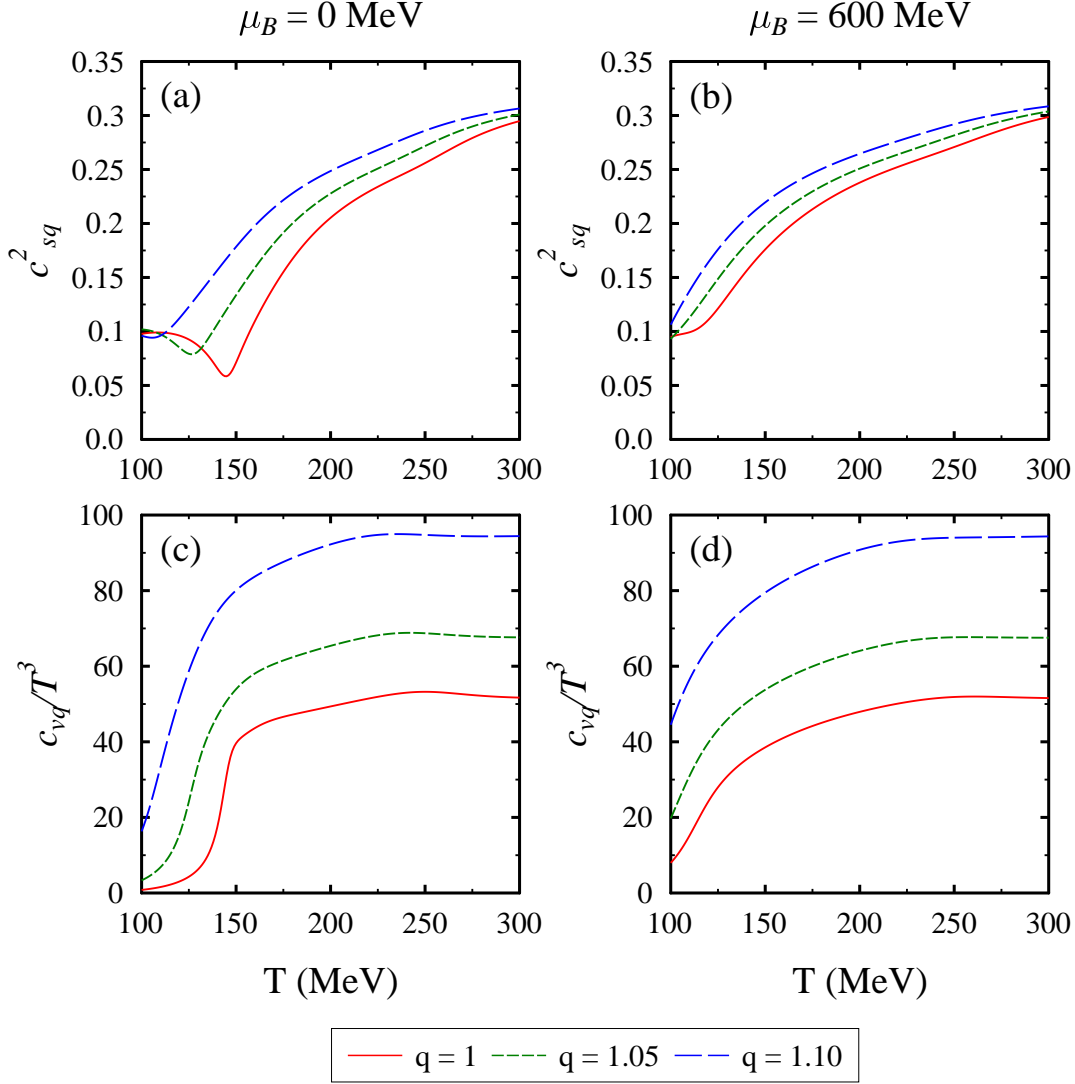


FIG. 5. The speed of sound squared c_{sq}^2 and scaled specific heat c_{vq}/T^3 as a function of temperature T for $q = 1, 1.05$, and 1.10 , at $\mu_B = 0$ MeV [in subplots (a) and (c)] and $\mu_B = 600$ MeV, $\mu_I = -30$ MeV, and $\mu_S = 125$ MeV [in subplots (b) and (d)].

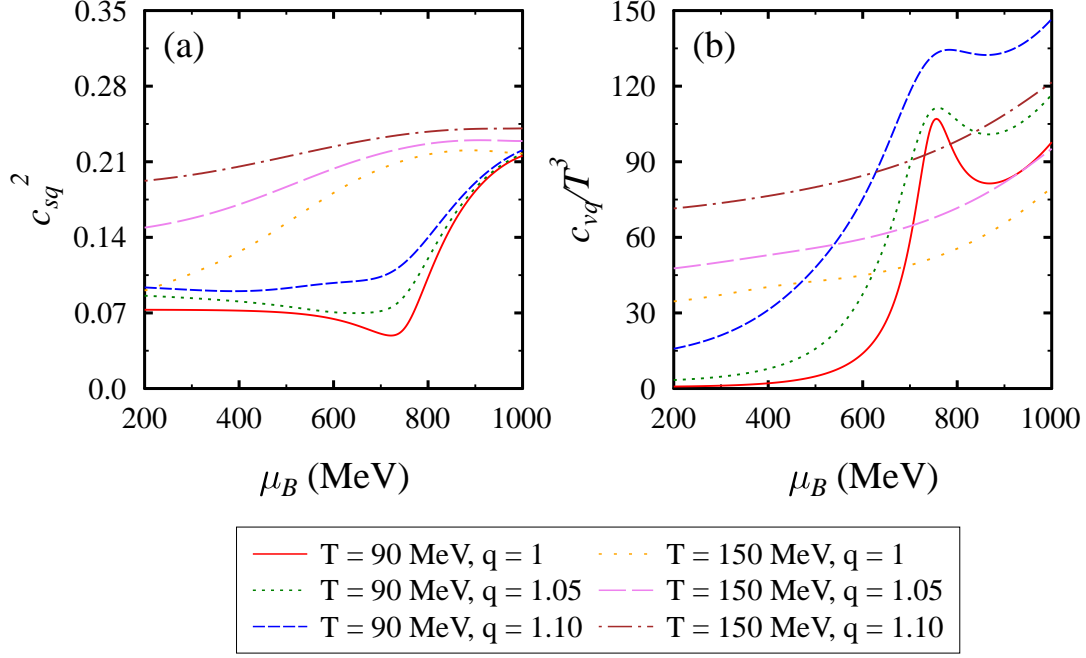


FIG. 6. The speed of sound squared c_{sq}^2 and scaled specific heat c_{vq}/T^3 as a function of baryon chemical potential μ_B for $q = 1, 1.05, \text{ and } 1.10$, at temperatures $T = 90$ and 150 MeV.

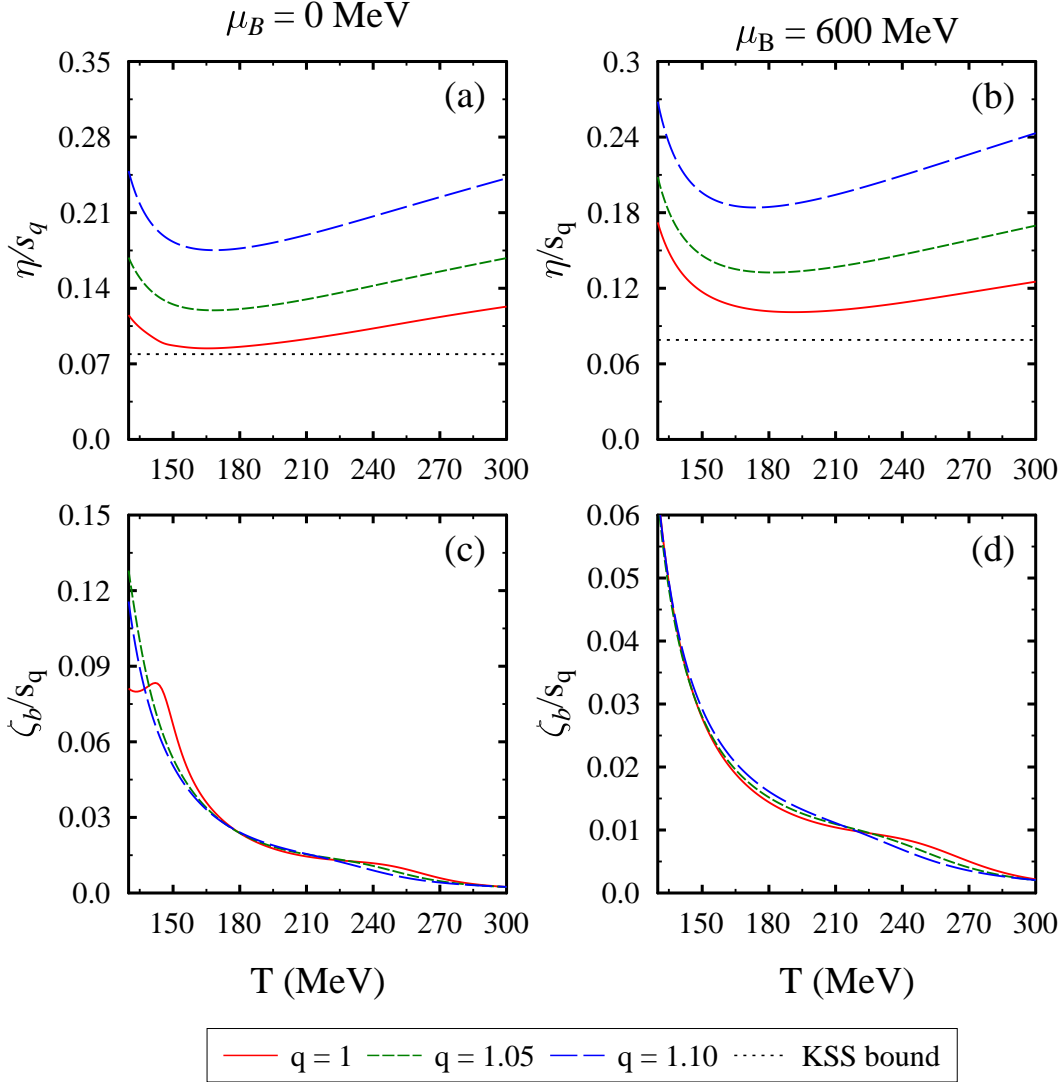


FIG. 7. The specific shear viscosity η/s_q and normalised bulk viscosity ζ_b/s_q as a function of temperature T for $q = 1, 1.05,$ and $1.10,$ at $\mu_B = 0$ MeV [in subplots (a) and (c)] and $\mu_B = 600$ MeV, $\mu_I = -30$ MeV, and $\mu_S = 125$ MeV [in subplots (b) and (d)].

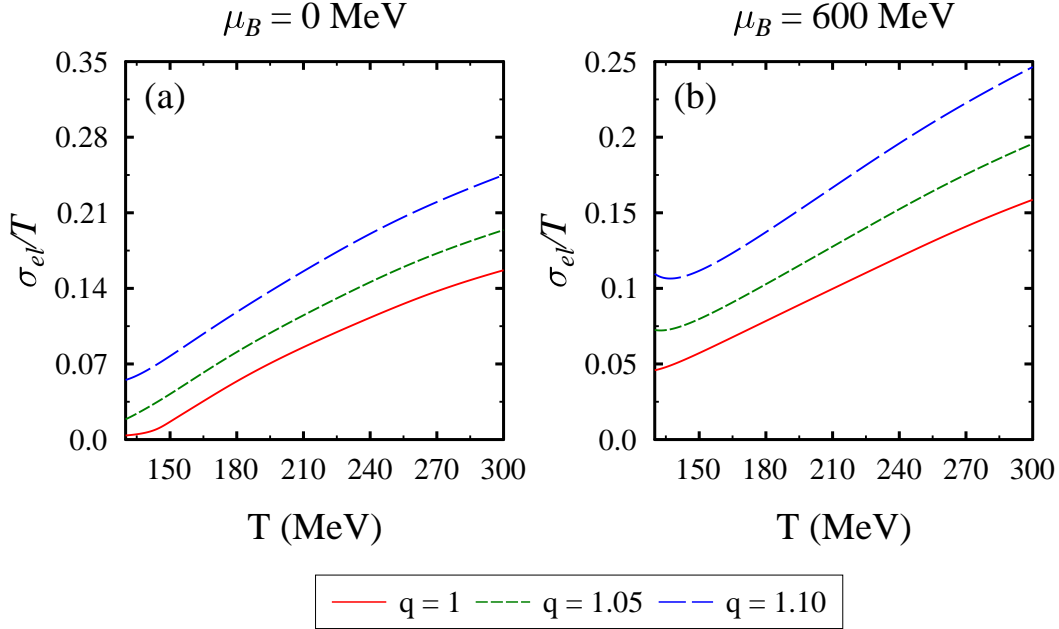


FIG. 8. The normalised electrical conductivity σ_{el}/T as a function of temperature T for $q = 1$, 1.05, and 1.10, at $\mu_B = 0$ MeV [in subplot (a)] and $\mu_B = 600$ MeV, $\mu_I = -30$ MeV, and $\mu_S = 125$ MeV [in subplot (b)].

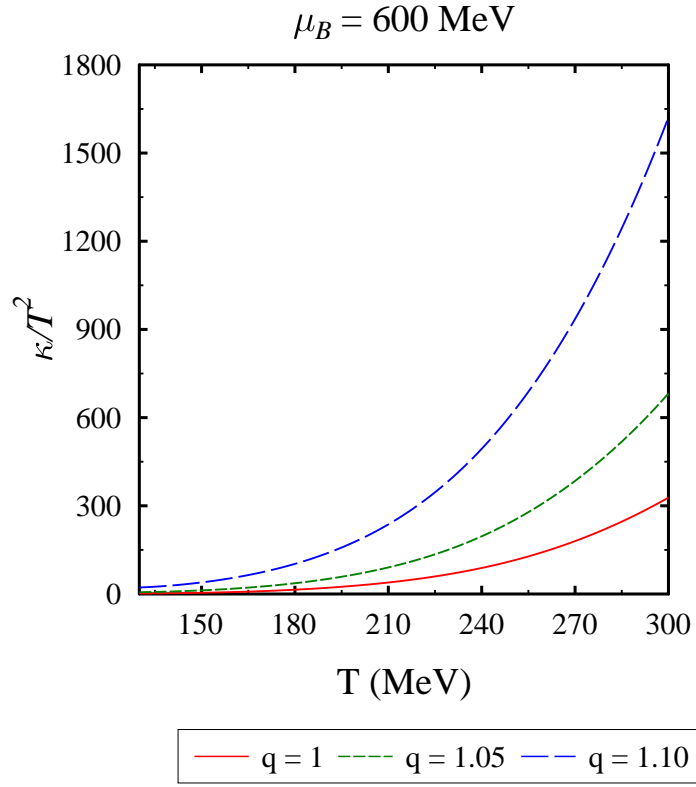


FIG. 9. The variation of normalised thermal conductivity κ/T^2 with temperature T for $q = 1$, 1.05, and 1.10, at $\mu_B = 600 \text{ MeV}$, $\mu_I = -30 \text{ MeV}$, and $\mu_S = 125 \text{ MeV}$

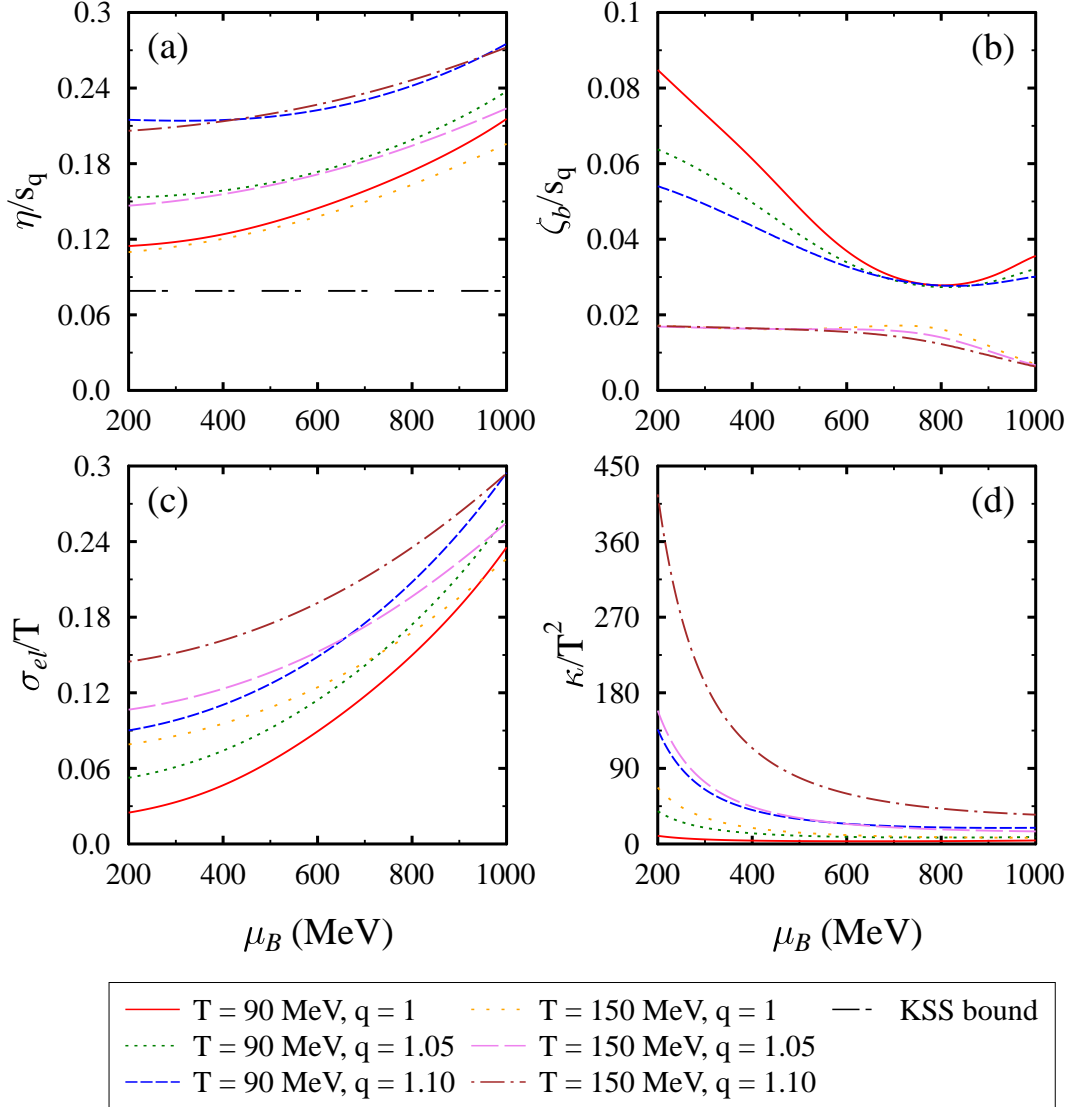


FIG. 10. The specific shear viscosity η/s_q , normalised bulk viscosity ζ_b/s_q , normalised electrical conductivity σ_{el}/T , and normalised thermal conductivity κ/T^2 as a function of baryon chemical potential μ_B for $q = 1, 1.05, \text{ and } 1.10$, at temperature $T = 90$ and 150 MeV.